Supplement of Atmos. Meas. Tech., 15, 407–433, 2022
https://doi.org/10.5194/amt-15-407-2022-supplement

Atmospheric Measurement Techniques
Open Access
EGU

Supplement of

Retrieval of aerosol properties using relative radiance measurements from an all-sky camera

Roberto Román et al.

Correspondence to: Roberto Román (robertor@goa.uva.es)

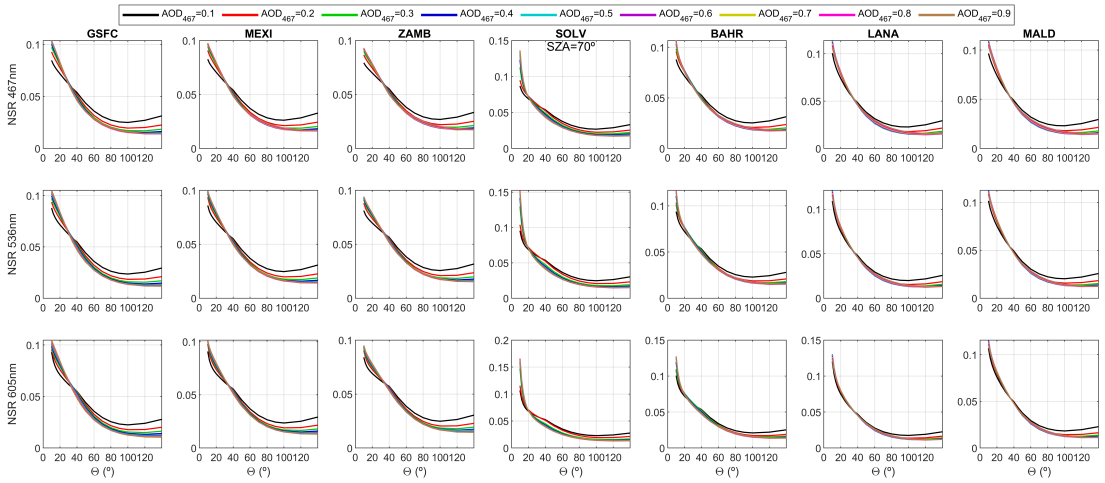

Figure S1. Normalized sky radiance (NSR) for solar zenith angle (SZA) of 70º at 467 nm (top row), 536 nm (middle row) and 605 nm (bottom row) as a function of scattering angle (Θ) for different AOD (at 467 nm) values and and for nine aerosol models.

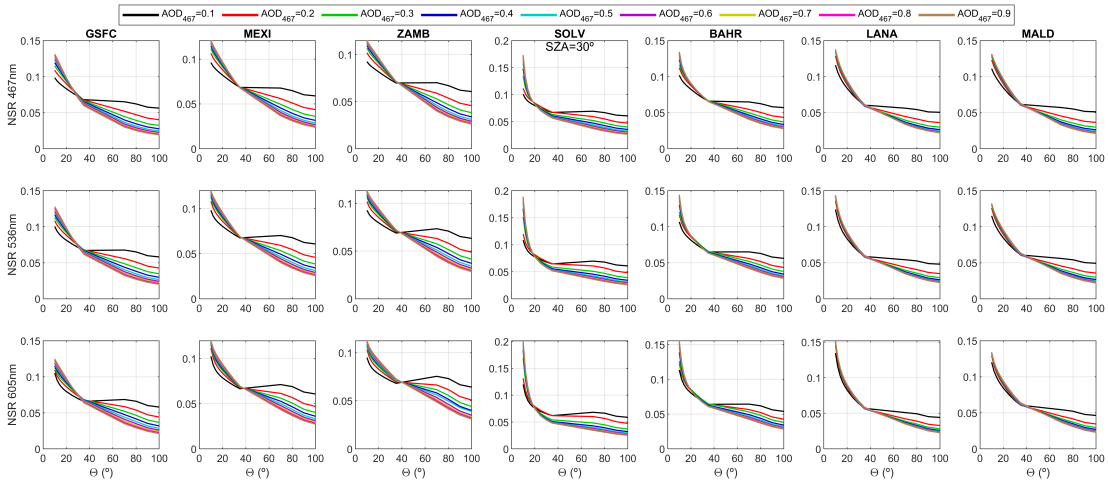

Figure S2. Normalized sky radiance (NSR) for solar zenith angle (SZA) of 30º at 467 nm (top row), 536 nm (middle row) and 605 nm (bottom row) as a function of scattering angle (Θ) for different AOD (at 467 nm) values and for nine aerosol models.

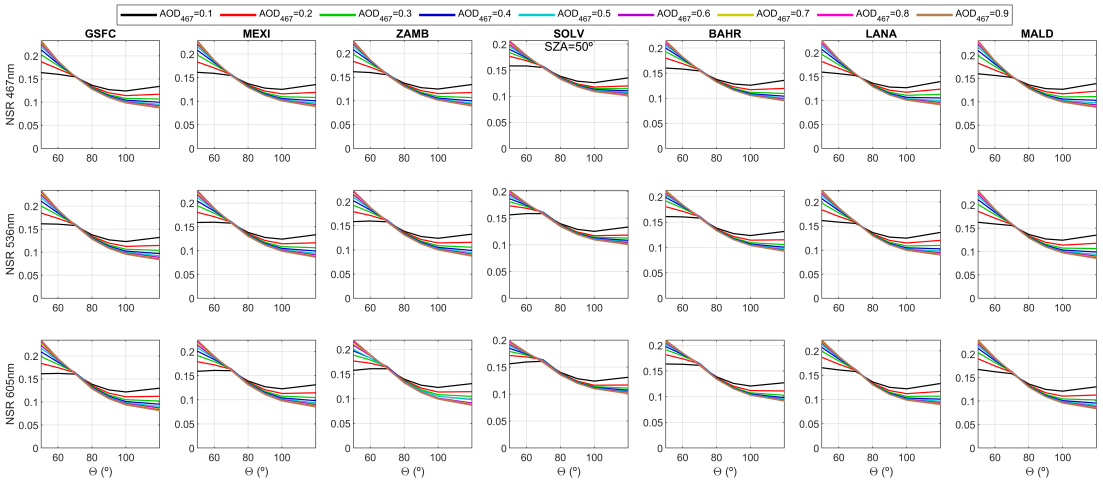

Figure S3. Normalized sky radiance (NSR) for solar zenith angle (SZA) of 50º at 467 nm (top row), 536 nm (middle row) and 605 nm (bottom row) as a function of scattering angle (Θ) for different AOD (at 467 nm) values and for nine aerosol models.

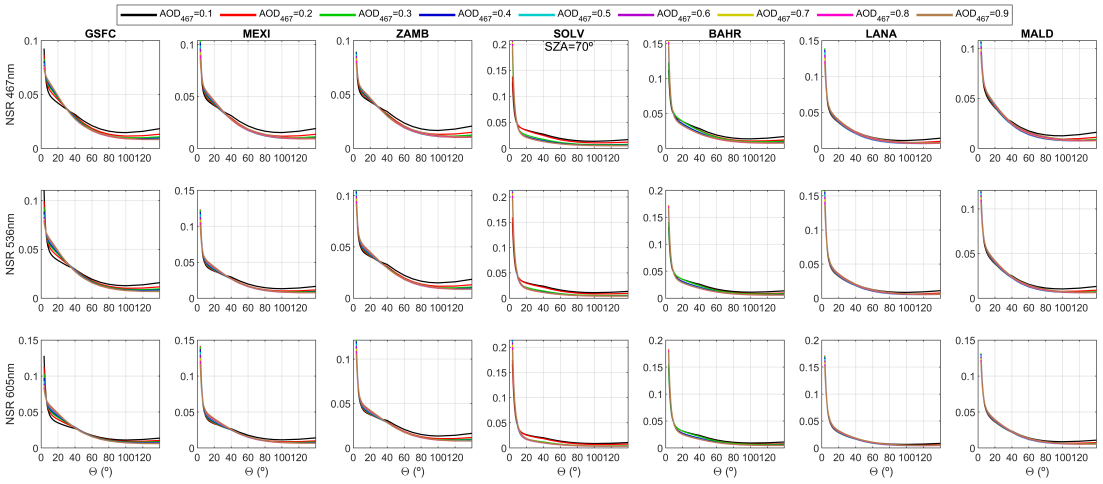

Figure S4. Normalized sky radiance (NSR) for solar zenith angle (SZA) of 70º at 467 nm (top row), 536 nm (middle row) and 605 nm (bottom row) as a function of scattering angle (Θ) for different AOD (at 467 nm) values and and for nine aerosol models. Scattering angles up to 3º instead of 10º are included.

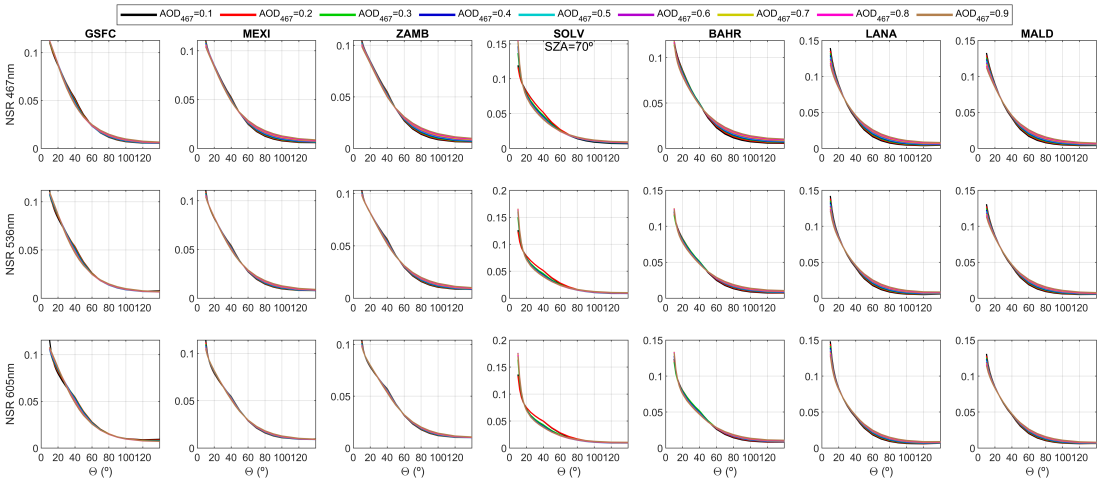

Figure S5. Normalized sky radiance (NSR) forsolar zenith angle (SZA) of 70º at 467 nm (top row), 536 nm (middle row) and 605 nm (bottom row) as a function of scattering angle (Θ) for different AOD (at 467 nm) values and for nine aerosol models under an atmosphere without Rayleigh scattering.

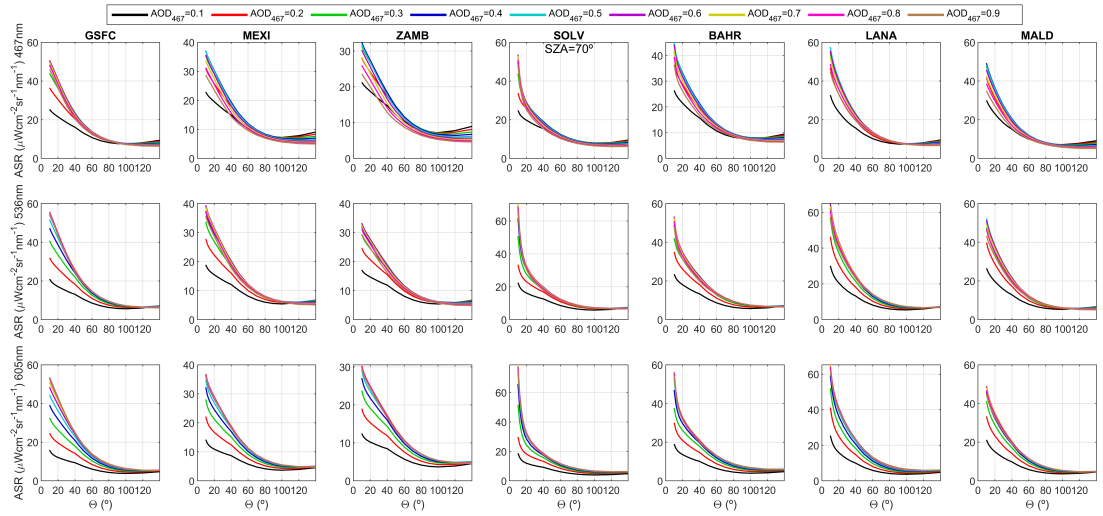

Figure S6. Absolute sky radiance (ASR) for solar zenith angle (SZA) of 70º at 467 nm (top row), 536 nm (middle row) and 605 nm (bottom row) as a function of scattering angle (Θ) for different AOD (at 467 nm) values and and for nine aerosol models.

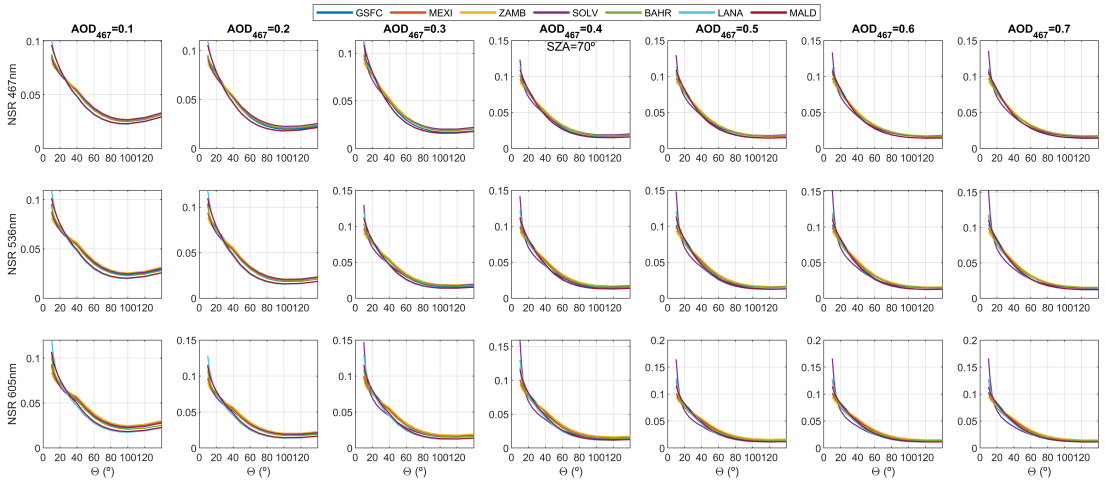

Figure S7. Normalized sky radiance (NSR) under solar zenith angle (SZA) of 70º at 467 nm (top row), 536 nm (middle row) and 605 nm (bottom row) as a function of scattering angle (Θ) for different aerosol models and AOD at 467 nm (AOD_{467}) values.

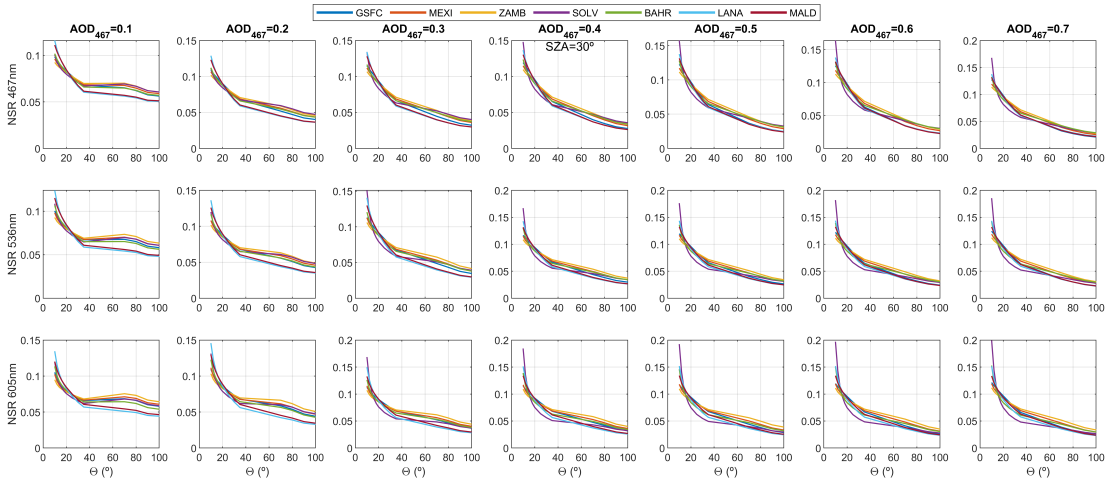

Figure S8. Normalized sky radiance (NSR) with a solar zenith angle (SZA) of 30º at 467 nm (top row), 536 nm (middle row) and 605 nm (bottom row) as a function of scattering angle (Θ) for different aerosol models and AOD at 467 nm (AOD_{467}) values.

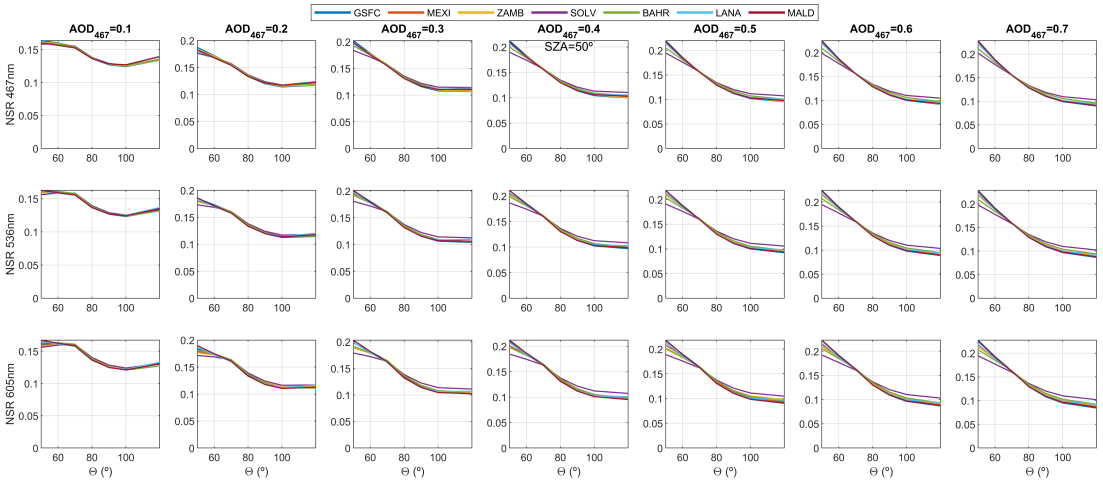

Figure S9. Normalized sky radiance (NSR) with a solar zenith angle (SZA) of 50º at 467 nm (top row), 536 nm (middle row) and 605 nm (bottom row) as a function of scattering angle (Θ) for different aerosol models and AOD at 467 nm (AOD_{467}) values.

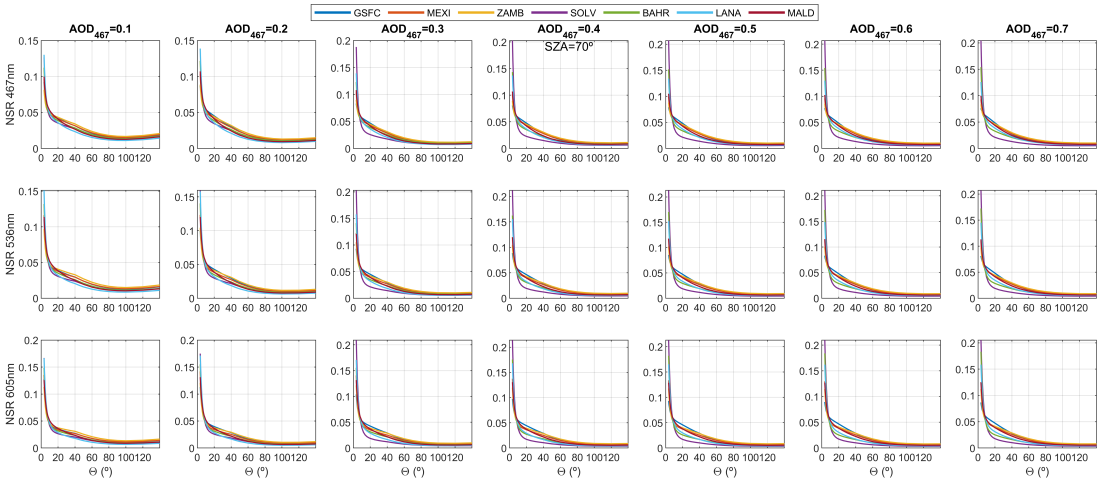

Figure S10. Normalized sky radiance (NSR) with a solar zenith angle (SZA) of 70º at 467 nm (top row), 536 nm (middle row) and 605 nm (bottom row) as a function of scattering angle (Θ) for different aerosol models and AOD at 467 nm (AOD_{467}) values. Scattering angles up to 3º instead of 10º are included.

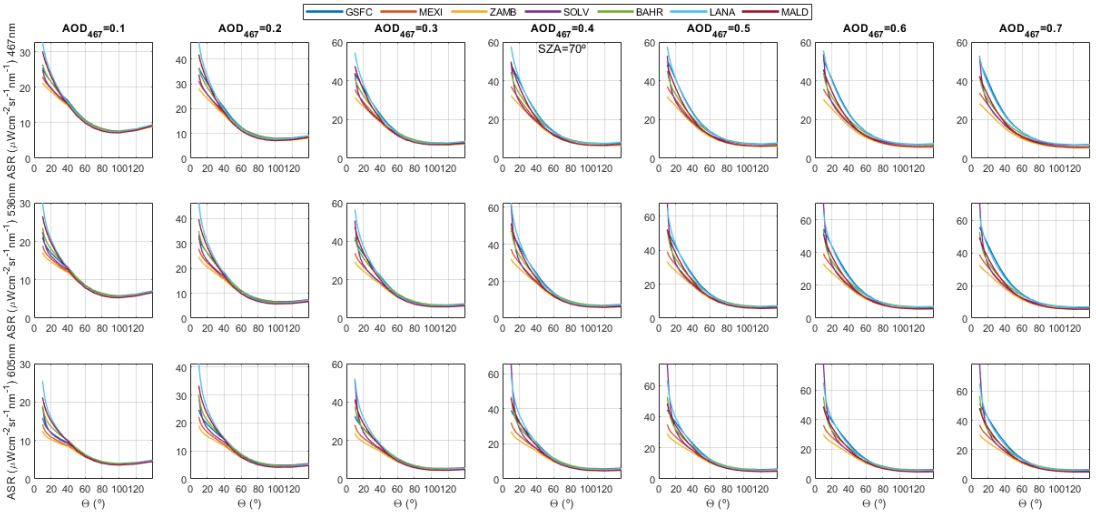

Figure S11. Absolute sky radiance (ASR) with a solar zenith angle (SZA) of 70º at 467 nm (top row), 536 nm (middle row) and 605 nm (bottom row) as a function of scattering angle (Θ) for different aerosol models and AOD at 467 nm (AOD_{467}) values.

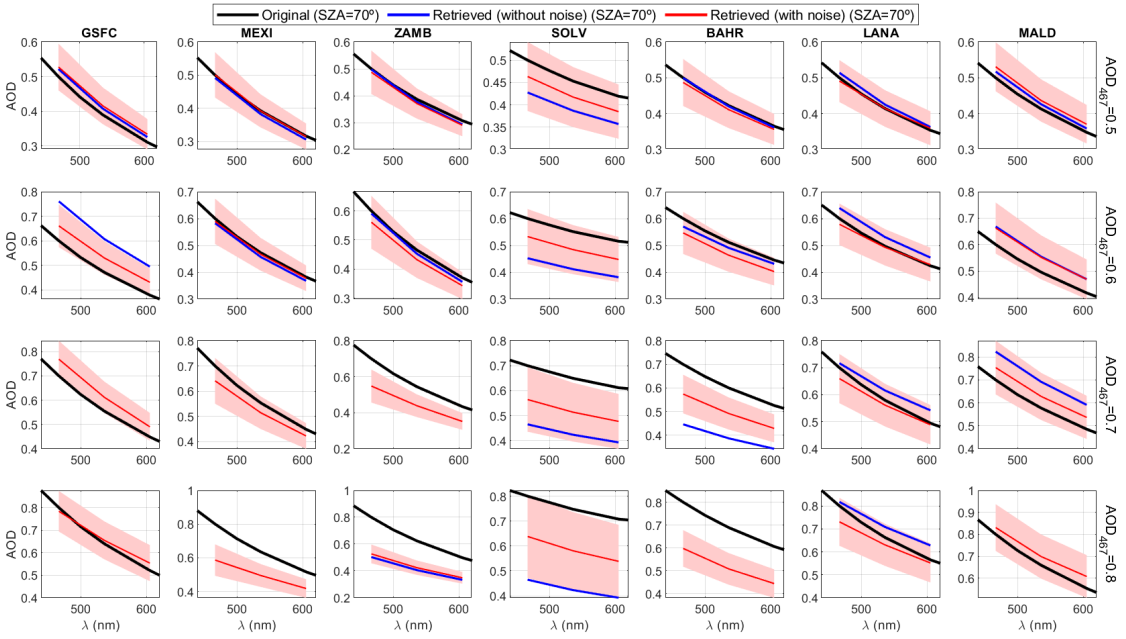

Figure S12. Aerosol optical depths (AODs) used as reference (black line), AODs retrieved without noise (blue line), and the median of all AODs retrieved with noise (red line) for solar zenith angle (SZA) equal to 70º. These AOD values are represented for different aerosol types (one type per column) and for AOD values at 467nm (AOD_{467}) of 0.5 (first row), 0.6 (second row), 0.7 (third row) and 0.8 (last row). Red shadowed-area corresponds to $\pm$ the standard deviation of all averaged size distributions retrieved with noise.

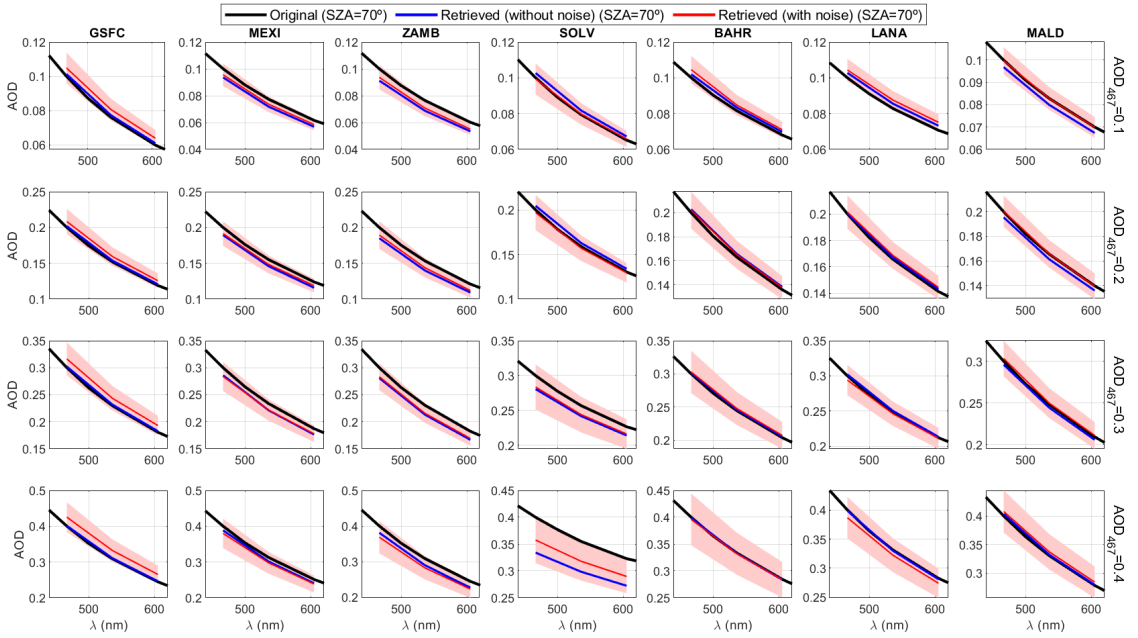

Figure S13. Aerosol optical depths (AODs) used as reference (black line), AODs retrieved without noise (blue line), and the median of all AODs retrieved with noise (red line) for solar zenith angle (SZA) equal to 70º. The retrievals have been done including scattering angles up to 3º instead of 10º. These AOD values are represented for different aerosol types (one type per column) and for AOD values at 467nm (AOD_{467}) of 0.1 (first row), 0.2 (second row), 0.3 (third row) and 0.4 (last row). Red shadowed-area corresponds to $\pm$ the standard deviation of all averaged size distributions retrieved with noise.

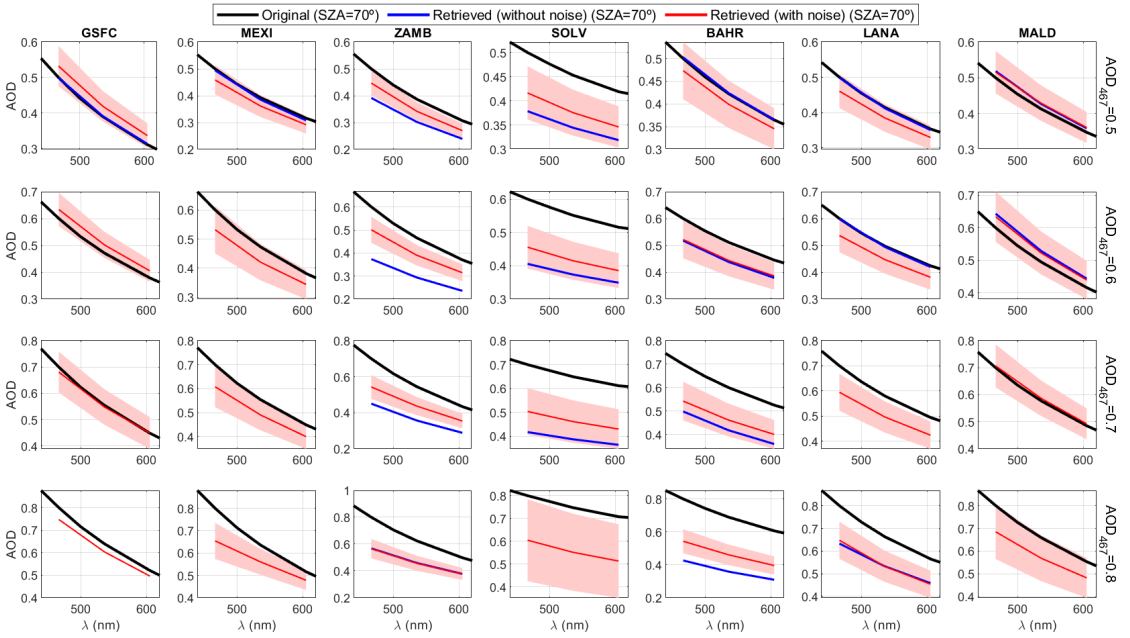

Figure S14. Aerosol optical depths (AODs) used as reference (black line), AODs retrieved without noise (blue line), and the median of all AODs retrieved with noise (red line) for solar zenith angle (SZA) equal to 70º. The retrievals have been done including scattering angles up to 3º instead of 10º. These AOD values are represented for different aerosol types (one type per column) and for AOD values at 467nm (AOD_{467}) of 0.5 (first row), 0.6 (second row), 0.7 (third row) and 0.8 (last row). Red shadowed-area corresponds to $\pm$ the standard deviation of all averaged size distributions retrieved with noise.

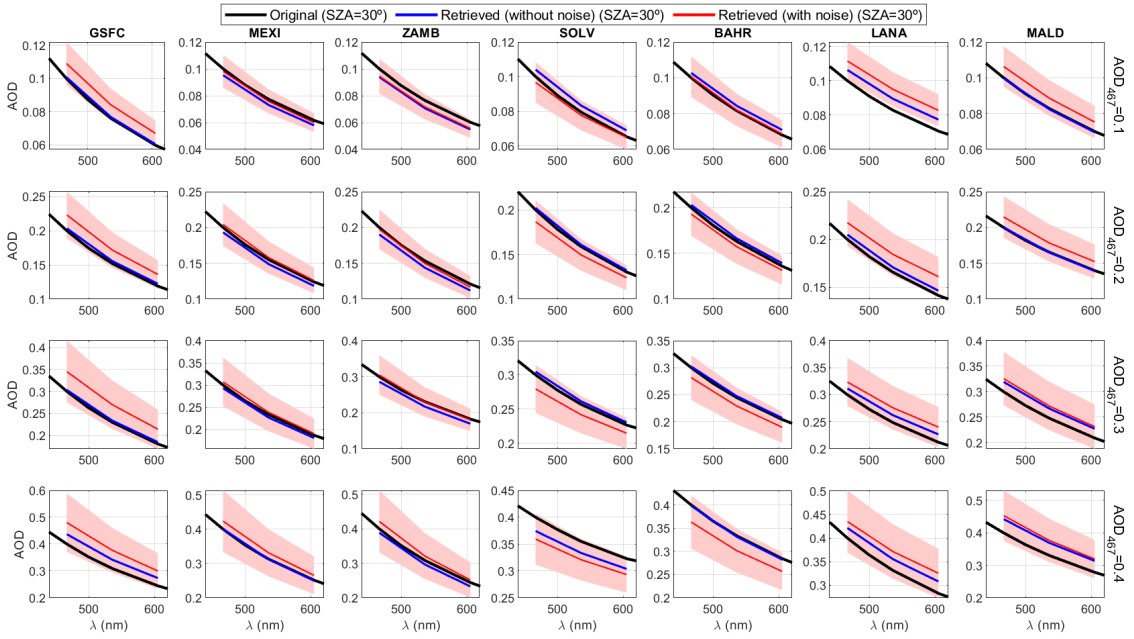

Figure S15. Aerosol optical depths (AODs) used as reference (black line), AODs retrieved without noise (blue line), and the median of all AODs retrieved with noise (red line) for solar zenith angle (SZA) equal to 30º. These AOD values are represented for different aerosol types (one type per column) and for AOD values at 467nm (AOD_{467}) of 0.1 (first row), 0.2 (second row), 0.3 (third row) and 0.4 (last row). Red shadowed-area corresponds to $\pm$ the standard deviation of all averaged size distributions retrieved with noise.

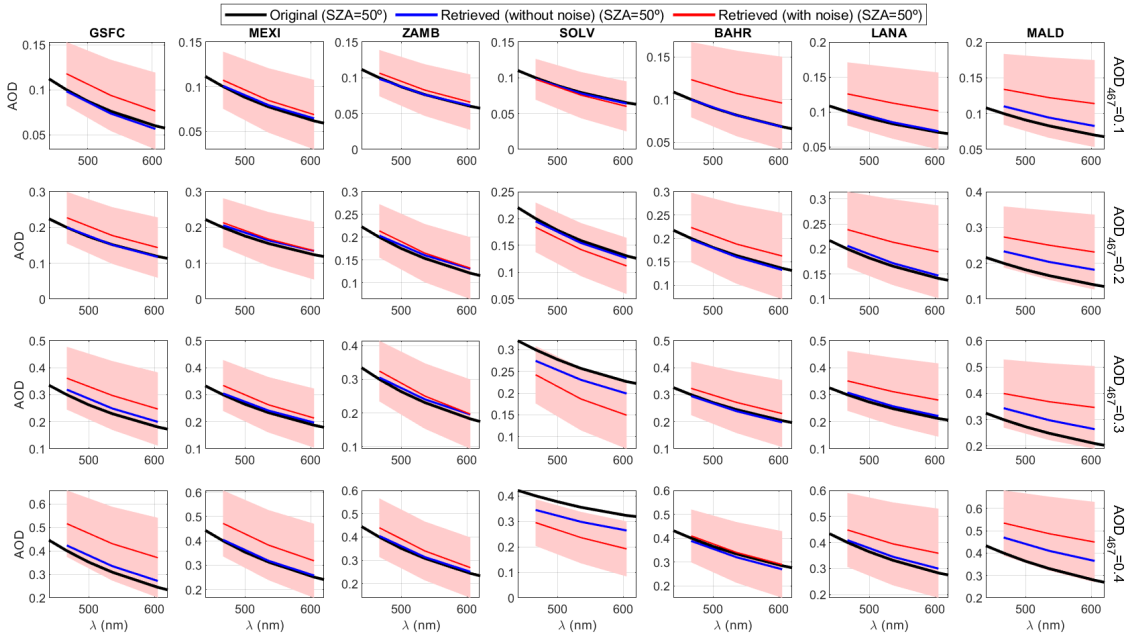

Figure S16. Aerosol optical depths (AODs) used as reference (black line), AODs retrieved without noise (blue line), and the median of all AODs retrieved with noise (red line) for solar zenith angle (SZA) equal to 50º. These AOD values are represented for different aerosol types (one type per column) and for AOD values at 467nm (AOD_{467}) of 0.1 (first row), 0.2 (second row), 0.3 (third row) and 0.4 (last row). Red shadowed-area corresponds to $\pm$ the standard deviation of all averaged size distributions retrieved with noise.

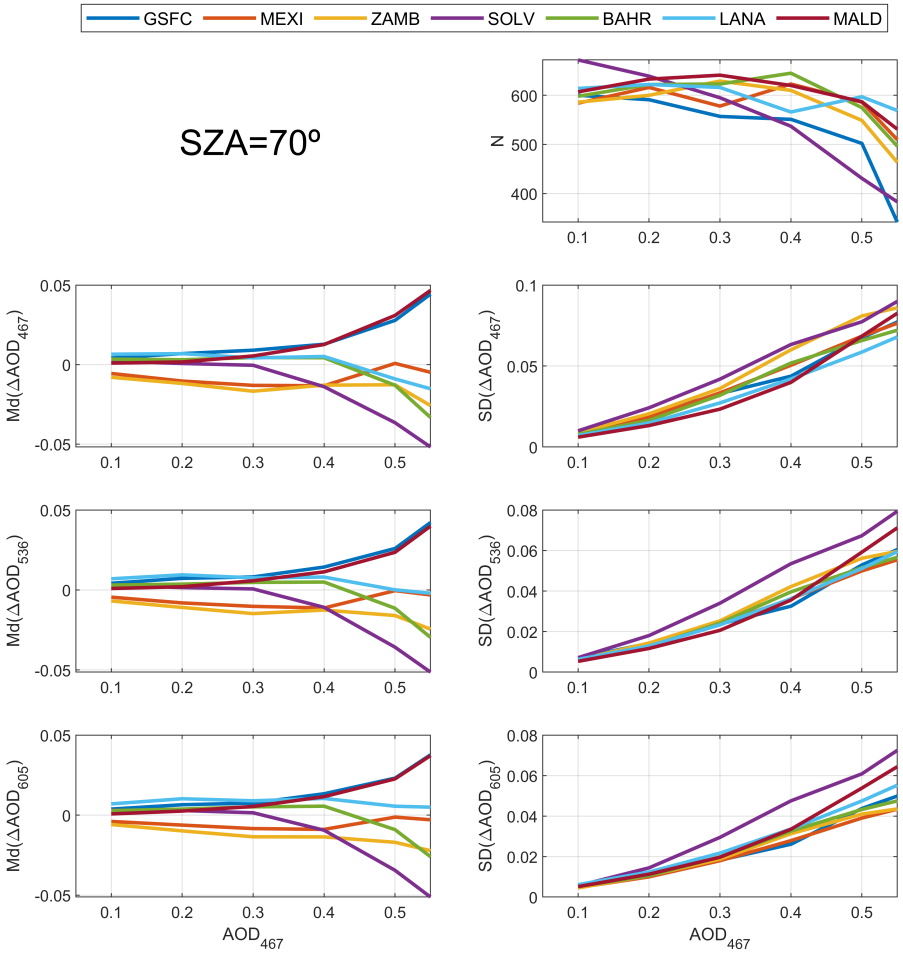

Figure S17. Median (Md) and standard deviation (SD) of the Δ differences between the available retrieved aerosol properties with noise and the original ones. The amount of available retrievals (N) is also shown. Only the retrievals under solar zenith angle (SZA) equal to 70º are used. The aerosol properties shown are aerosol optical depth (AOD) at 467 nm (AOD_{467}), 536 nm (AOD_{536}) and 605 nm (AOD_{605}). These Md and STD values are represented as a function of AOD_{467} for different aerosol types. x-axis goes from 0 to 0.5 to a better observation of this range.

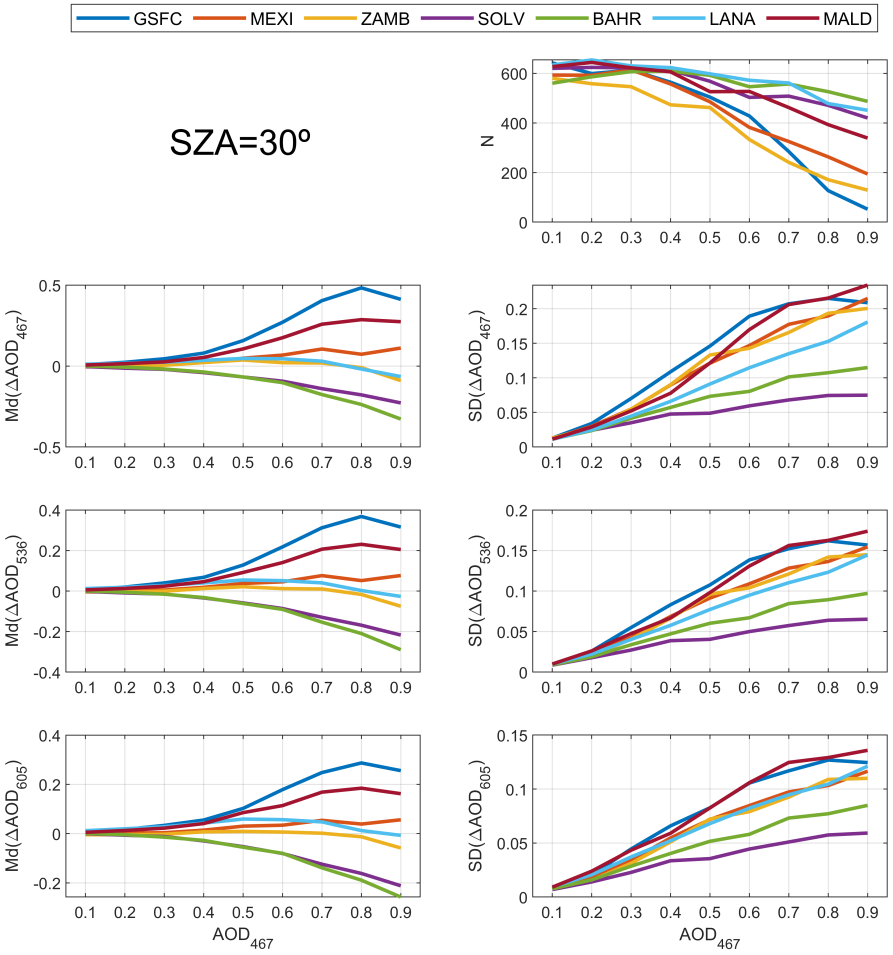

Figure S18. Median (Md) and standard deviation (SD) of the Δ differences between the available retrieved aerosol properties with noise and the original ones. The amount of available retrievals (N) is also shown. Only the retrievals under solar zenith angle (SZA) equal to 30º are used. The aerosol properties shown are aerosol optical depth (AOD) at 467 nm (AOD_{467}), 536 nm (AOD_{536}) and 605 nm (AOD_{605}). These Md and STD values are represented as a function of AOD_{467} for different aerosol types.

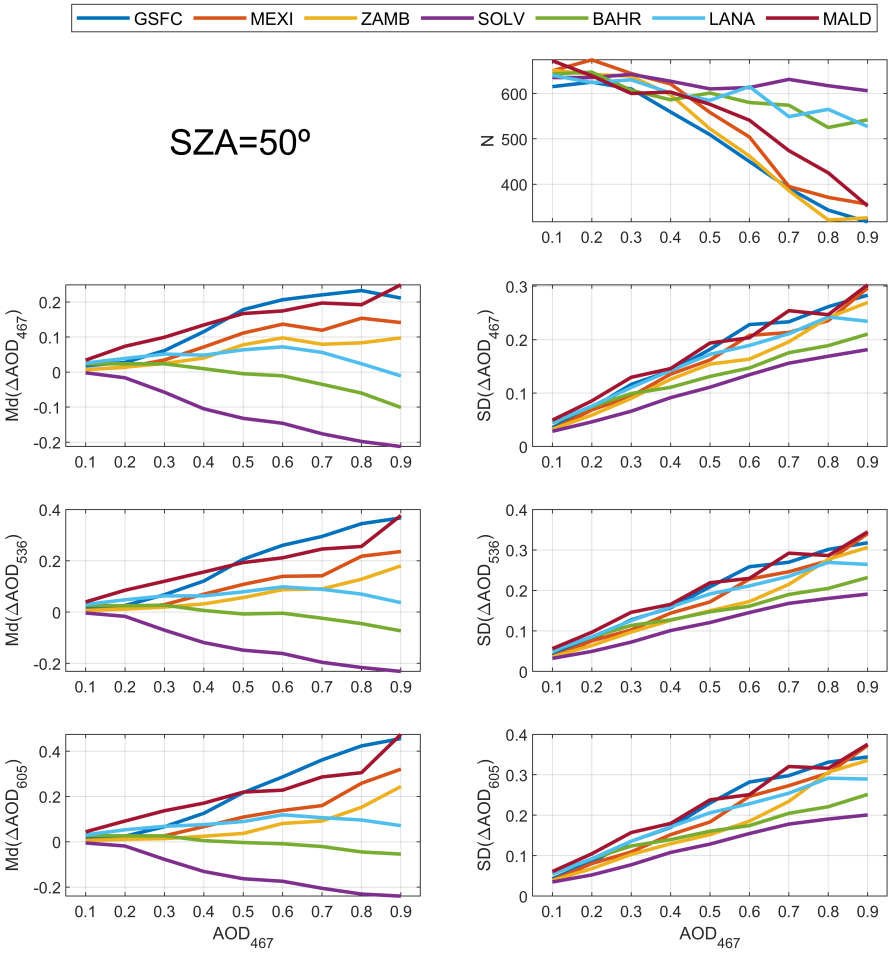

Figure S19. Median (Md) and standard deviation (SD) of the Δ differences between the available retrieved aerosol properties with noise and the original ones. The amount of available retrievals (N) is also shown. Only the retrievals under solar zenith angle (SZA) equal to 50º are used. TThe aerosol properties shown are aerosol optical depth (AOD) at 467 nm (AOD_{467}), 536 nm (AOD_{536}) and 605 nm (AOD_{605}). These Md and STD values are represented as a function of AOD_{467} for different aerosol types.

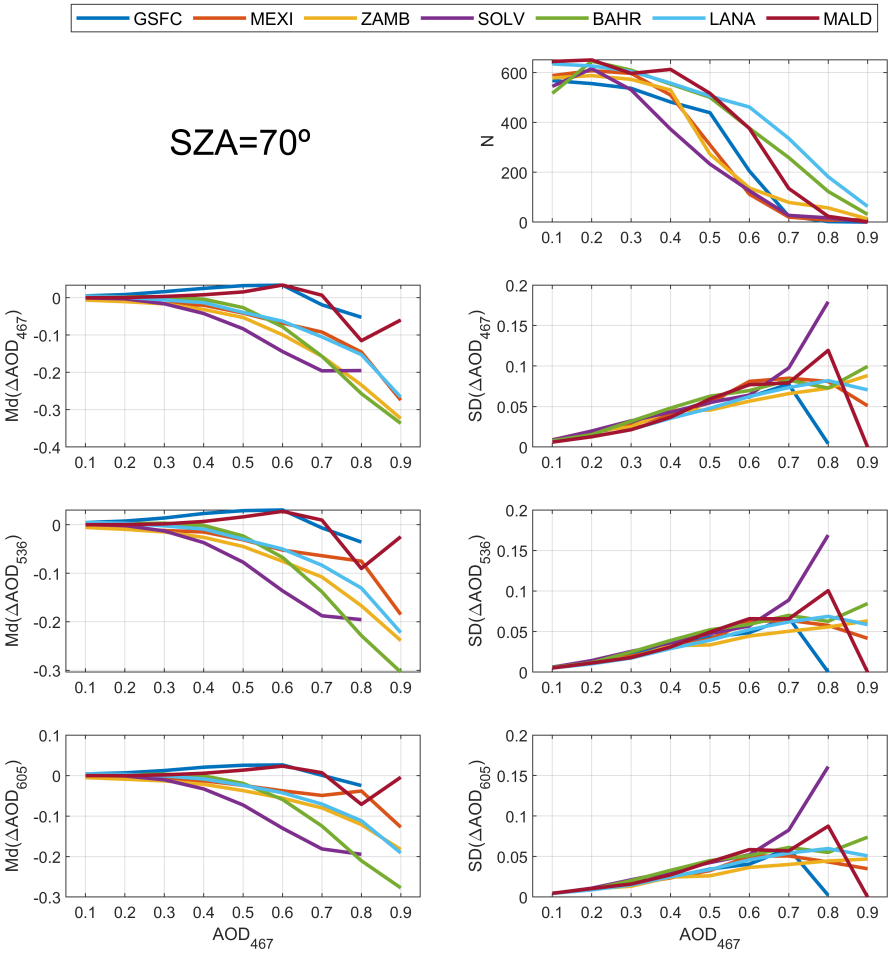

Figure S20. Median (Md) and standard deviation (SD) of the Δ differences between the available retrieved aerosol properties with noise and the original ones. The amount of available retrievals (N) is also shown. Only the retrievals under solar zenith angle (SZA) equal to 70º are used. The aerosol properties shown are aerosol optical depth (AOD) at 467 nm (AOD_{467}), 536 nm (AOD_{536}) and 605 nm (AOD_{605}). These Md and STD values are represented as a function of AOD_{467} for different aerosol types. The retrievals have been done including scattering angles up to 3º instead of 10º.

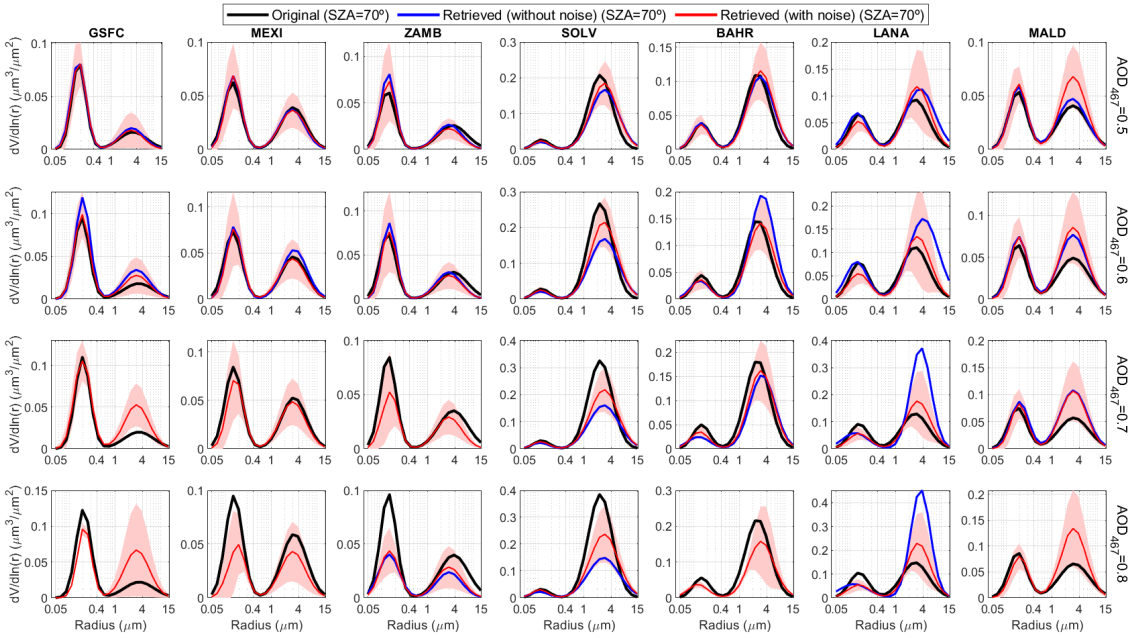

Figure S21. Original size distribution used as reference (black line), size distribution retrieved without noise (blue line), and the median of all retrieved size distributions with noise (red line) for a solar zenith angle (SZA) equal to 70º. These size distributions are represented for different aerosol types (one type per column) and for values of AOD (aerosol optical depth) at 467nm (AOD_{467}) of 0.5 (first row), 0.6 (second row), 0.7 (third row) and 0.8 (last row). Red shadowed area corresponds to $\pm$ the standard deviation of all averaged size distributions retrieved with noise.

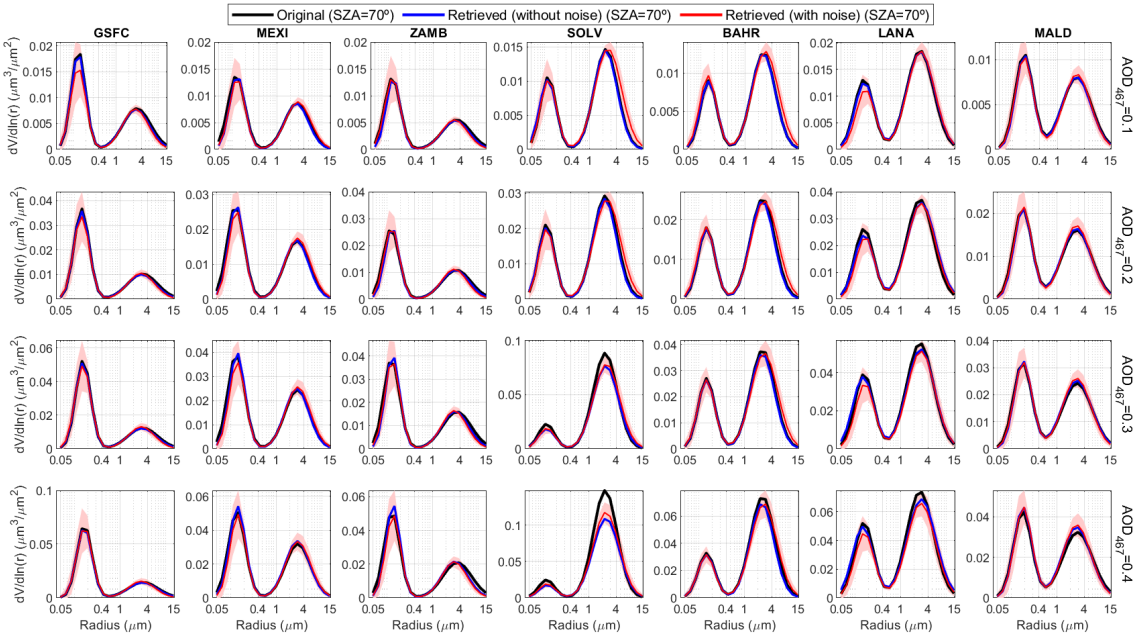

Figure S22. Original size distribution used as reference (black line), size distribution retrieved without noise (blue line), and the median of all retrieved size distributions with noise (red line) for a solar zenith angle (SZA) equal to 70º. The retrievals have been done including scattering angles up to 3º instead of 10º. These size distributions are represented for different aerosol types (one type per column) and for values of AOD (aerosol optical depth) at 467nm (AOD_{467}) of 0.1 (first row), 0.2 (second row), 0.3 (third row) and 0.4 (last row). Red shadowed area corresponds to $\pm$ the standard deviation of all averaged size distributions retrieved with noise.

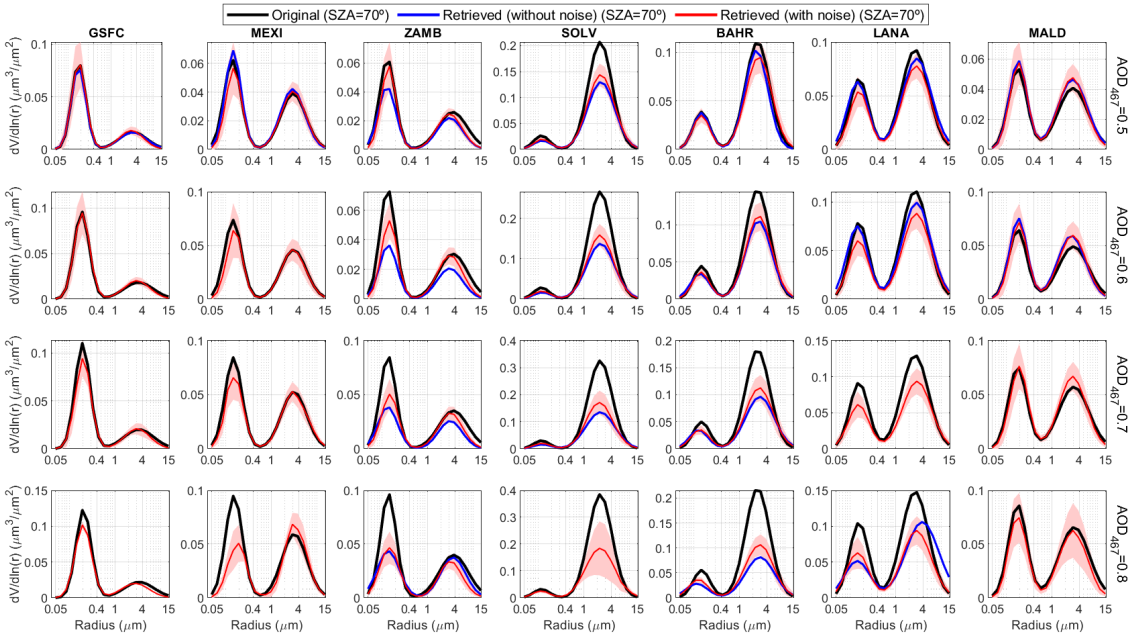

Figure S23. Original (black line), retrieved without noise (blue line), and median of all retrieved with noise (red line) aerosol volume size distributions under solar zenith angle (SZA) equal to 70º. The retrievals have been done including scattering angles up to 3º instead of 10º. These size distributions are represented for different aerosol types (one type per column) and for values of AOD (aerosol optical depth) at 467nm (AOD_{467}) of 0.5 (first row), 0.6 (second row), 0.7 (third row) and 0.8 (last row). Red shadowed area corresponds to $\pm$ the standard deviation of all averaged size distributions retrieved with noise.

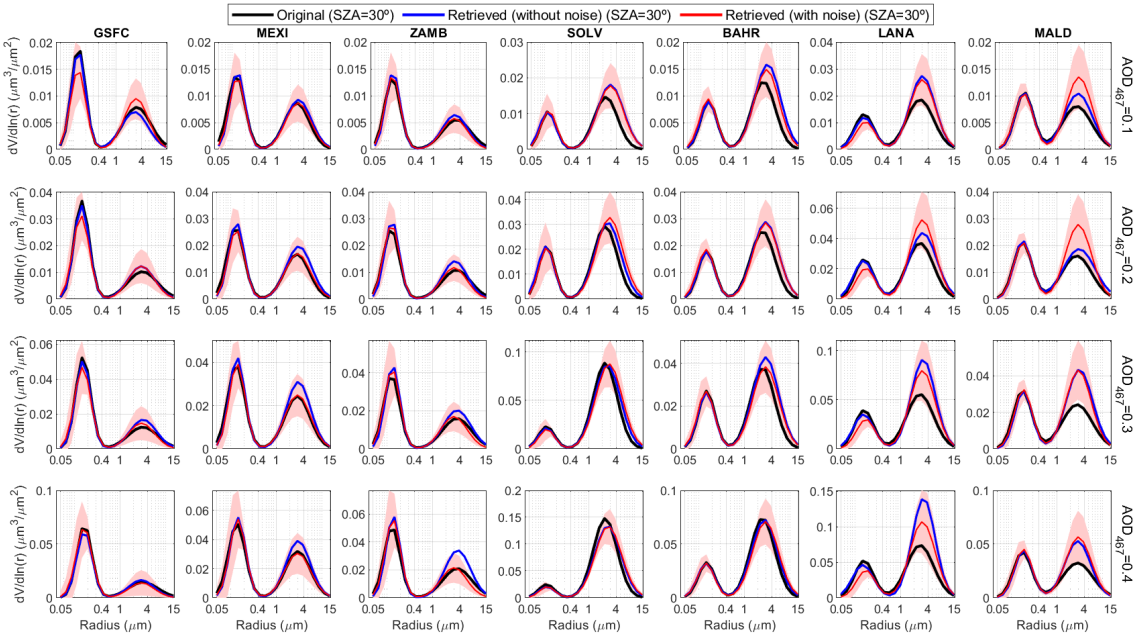

Figure S24. Original size distribution used as reference (black line), size distribution retrieved without noise (blue line), and the median of all retrieved size distributions with noise (red line) for a solar zenith angle (SZA) equal to 30º. These size distributions are represented for different aerosol types (one type per column) and for values of AOD (aerosol optical depth) at 467nm (AOD_{467}) of 0.1 (first row), 0.2 (second row), 0.3 (third row) and 0.4 (last row). Red shadowed area corresponds to $\pm$ the standard deviation of all averaged size distributions retrieved with noise.

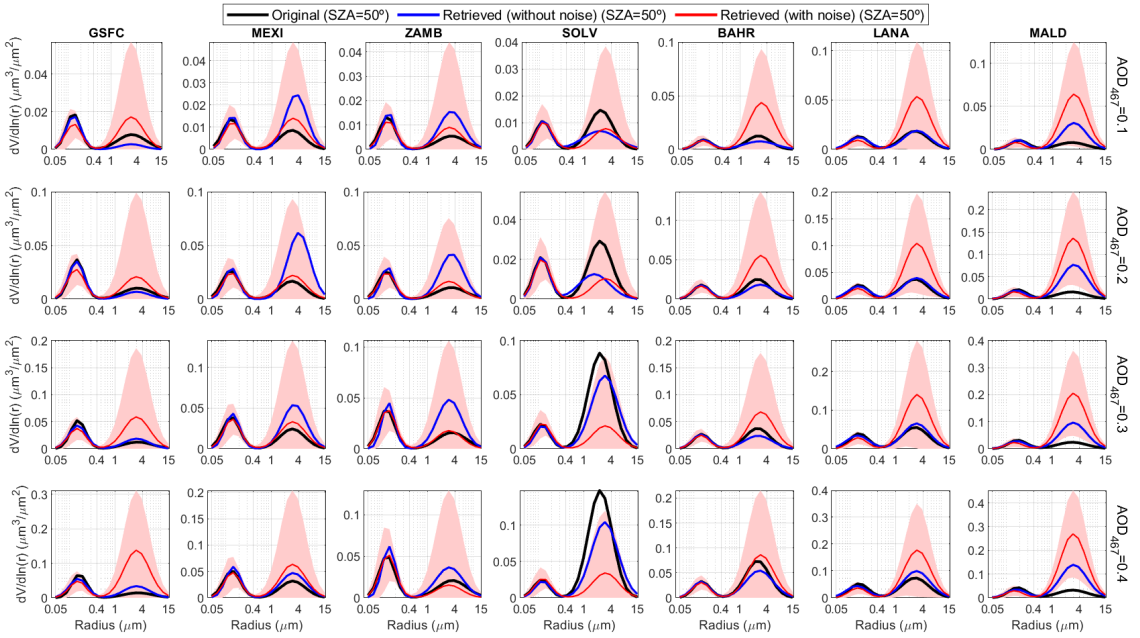

Figure S25. Original size distribution used as reference (black line), size distribution retrieved without noise (blue line), and the median of all retrieved size distributions with noise (red line) for a solar zenith angle (SZA) equal to 50º. These size distributions are represented for different aerosol types (one type per column) and for values of AOD (aerosol optical depth) at 467nm (AOD_{467}) of 0.1 (first row), 0.2 (second row), 0.3 (third row) and 0.4 (last row). Red shadowed area corresponds to $\pm$ the standard deviation of all averaged size distributions retrieved with noise.

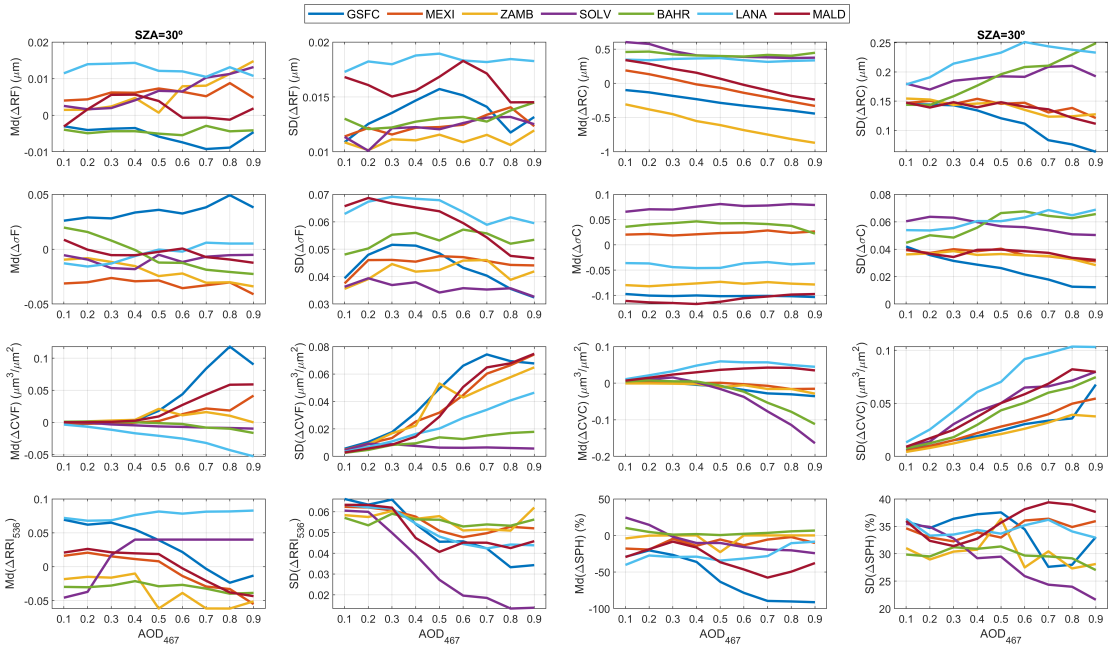

Figure S26. Median (Md) and standard deviation (SD) of the Δ differences between the available retrieved aerosol properties with noise and the original ones under solar zenith angle (SZA) of 30º. The aerosol properties are volume median radius of fine (RF) and coarse (RC) modes, standard deviation of log-normal distribution for fine (σF) and coarse (σC) modes, aerosol volume concentration for fine (VCF) and coarse (VCC) modes, real part of refractive index at 536 nm (RRI_{536}), and the fraction of spherical particles (SPH). These Md and STD values are represented as a function of AOD_{467} for different aerosol types.

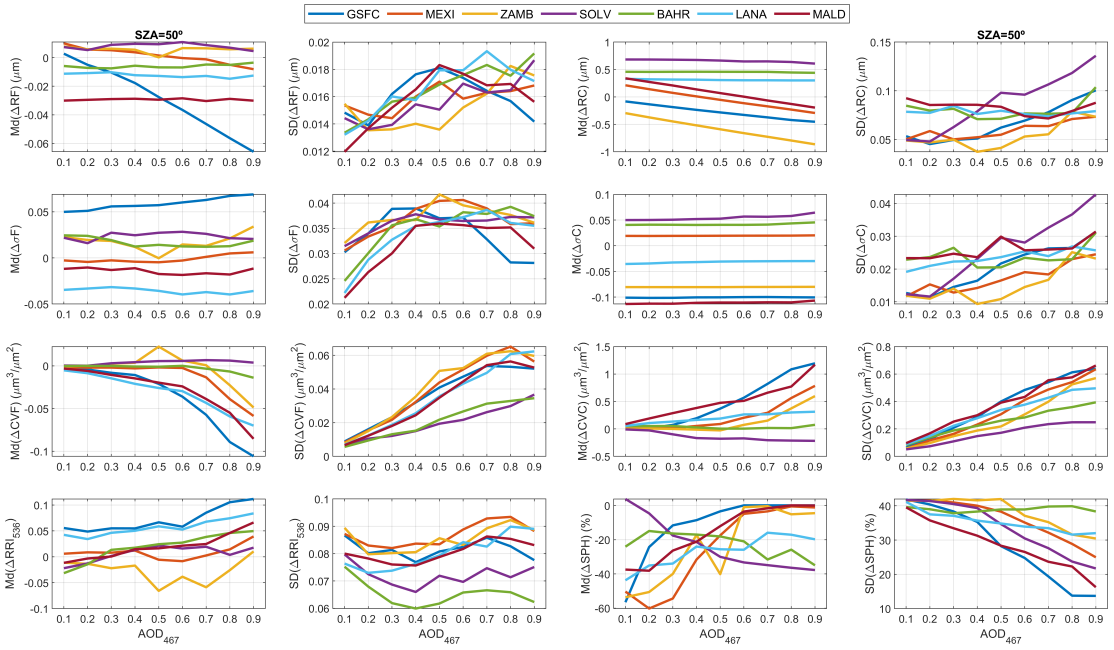

Figure S27. Median (Md) and standard deviation (SD) of the Δ differences between the available retrieved aerosol properties with noise and the original ones under solar zenith angle (SZA) of 50º. The aerosol properties are volume median radius of fine (RF) and coarse (RC) modes, standard deviation of log-normal distribution for fine (σF) and coarse (σC) modes, aerosol volume concentration for fine (VCF) and coarse (VCC) modes, real part of refractive index at 536 nm (RRI_{536}), and the fraction of spherical particles (SPH). These Md and STD values are represented as a function of AOD_{467} for different aerosol types.

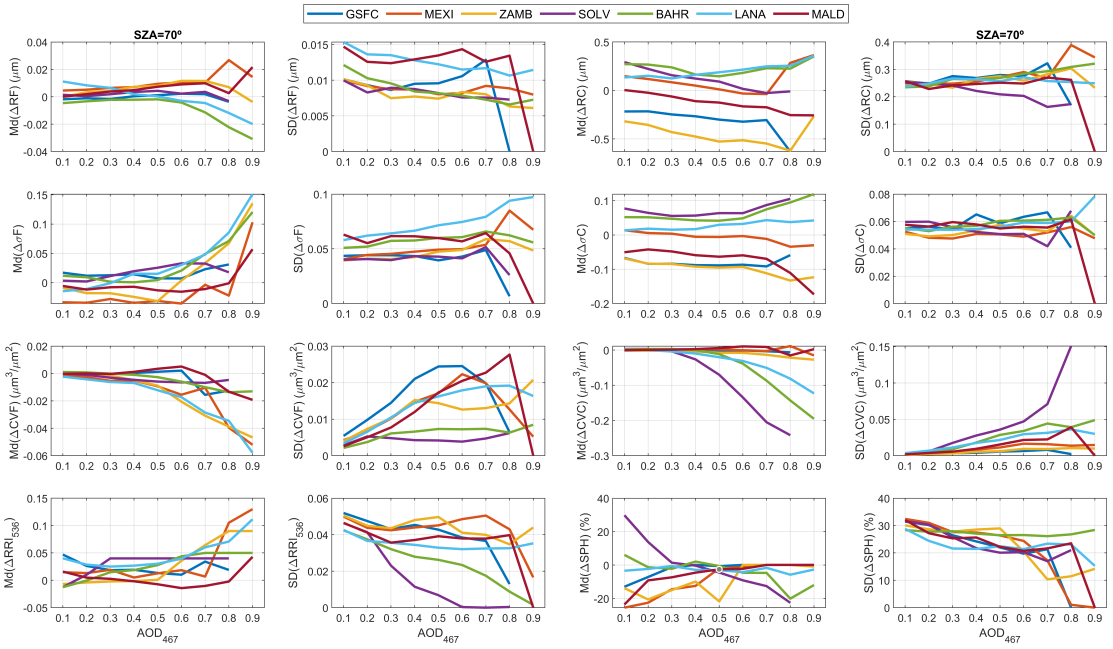

Figure S28. Median (Md) and standard deviation (SD) of the Δ differences between the available retrieved aerosol properties with noise and the original ones under solar zenith angle (SZA) of 70º. The retrievals have been done including scattering angles up to 3º instead of 10º. The aerosol properties are volume median radius of fine (RF) and coarse (RC) modes, standard deviation of log-normal distribution for fine (σF) and coarse (σC) modes, aerosol volume concentration for fine (VCF) and coarse (VCC) modes, real part of refractive index at 536 nm (RRI_{536}), and the fraction of spherical particles (SPH). These Md and STD values are represented as a function of AOD_{467} for different aerosol types.

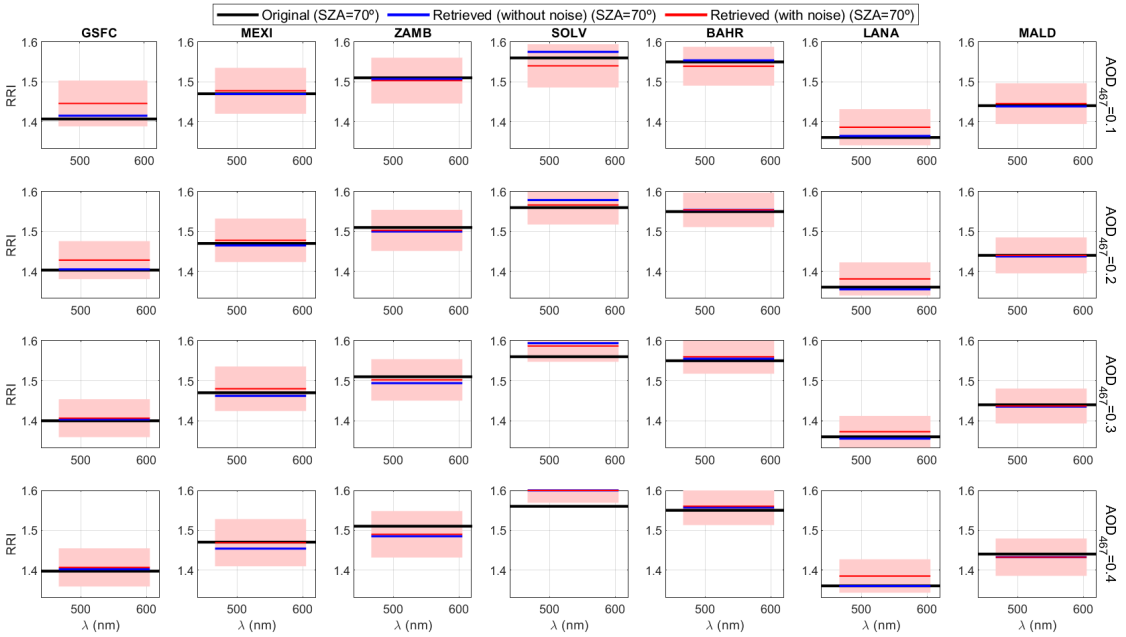

Figure S29. Original real part of refractive indices (RRI) used as reference (black line), RRI retrieved without noise (blue line), and the median of all retrieved RRIs with noise (red line) for a solar zenith angle (SZA) equal to 70º. These AOD values are represented for different aerosol types (one type per column) and for AOD values at 467nm (AOD_{467}) of 0.1 (first row), 0.2 (second row), 0.3 (third row) and 0.4 (last row). Red shadowed area corresponds to $\pm$ the standard deviation of all averaged size distributions retrieved with noise.

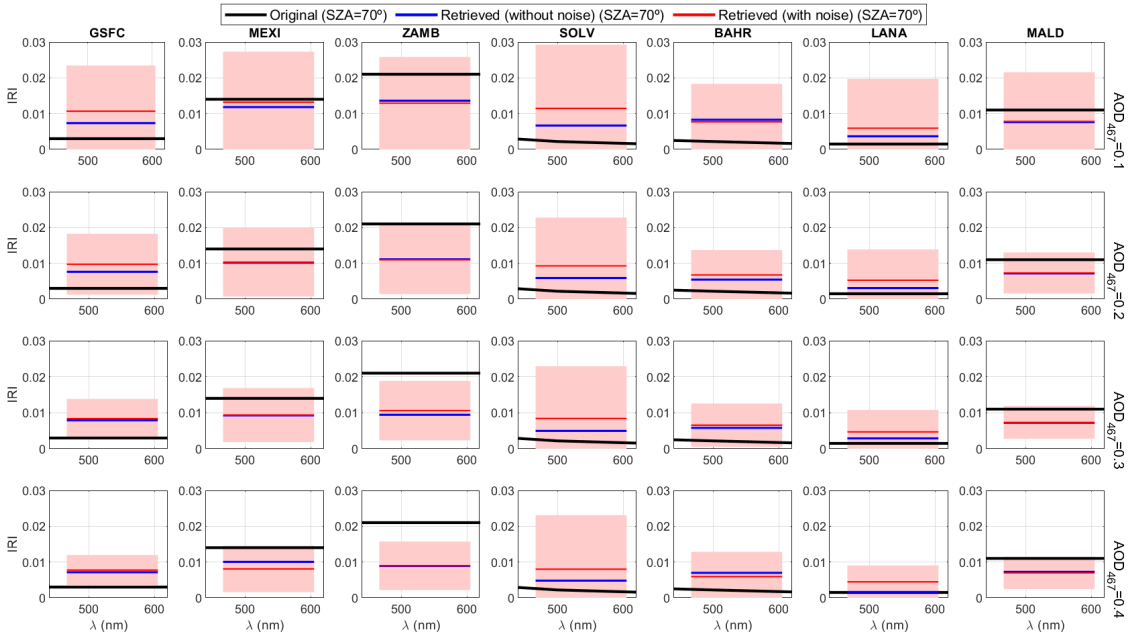

Figure S30. Original imaginary part of refractive indices (IRI) used as reference (black line), IRI retrieved without noise (blue line), and the median of all retrieved IRIs with noise (red line) for a solar zenith angle (SZA) equal to 70º. These AOD values are represented for different aerosol types (one type per column) and for AOD values at 467nm (AOD_{467}) of 0.1 (first row), 0.2 (second row), 0.3 (third row) and 0.4 (last row). Red shadowed area corresponds to $\pm$ the standard deviation of all averaged size distributions retrieved with noise. These results are obtained assuming IRI as an additional parameter to be retrieved in GRASP-CAM configuration.

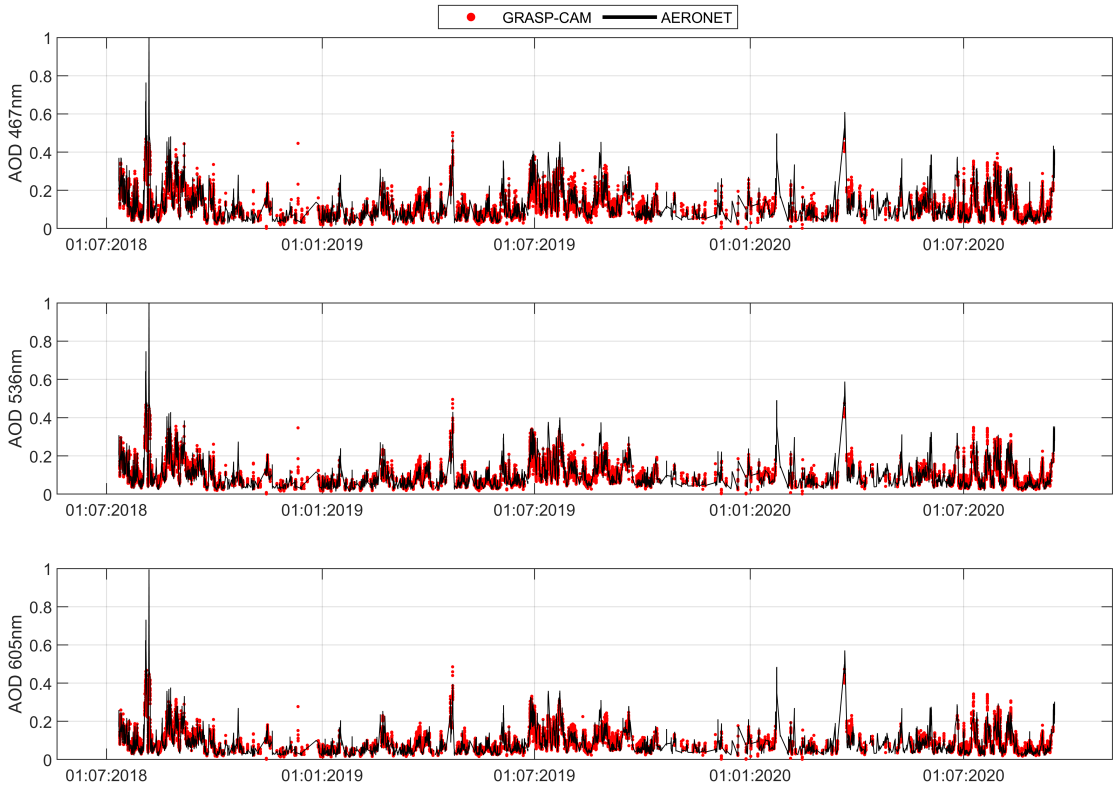

Figure S31. Aerosol optical depth (AOD) at 467 nm (upper panel), 536 nm (middle panel) and 605 nm (bottom panel) retrieved by GRASP with the single-pixel approach (GRASP-CAM) and by AERONET at Valladolid from 11 July 2018 to 15 September 2020.

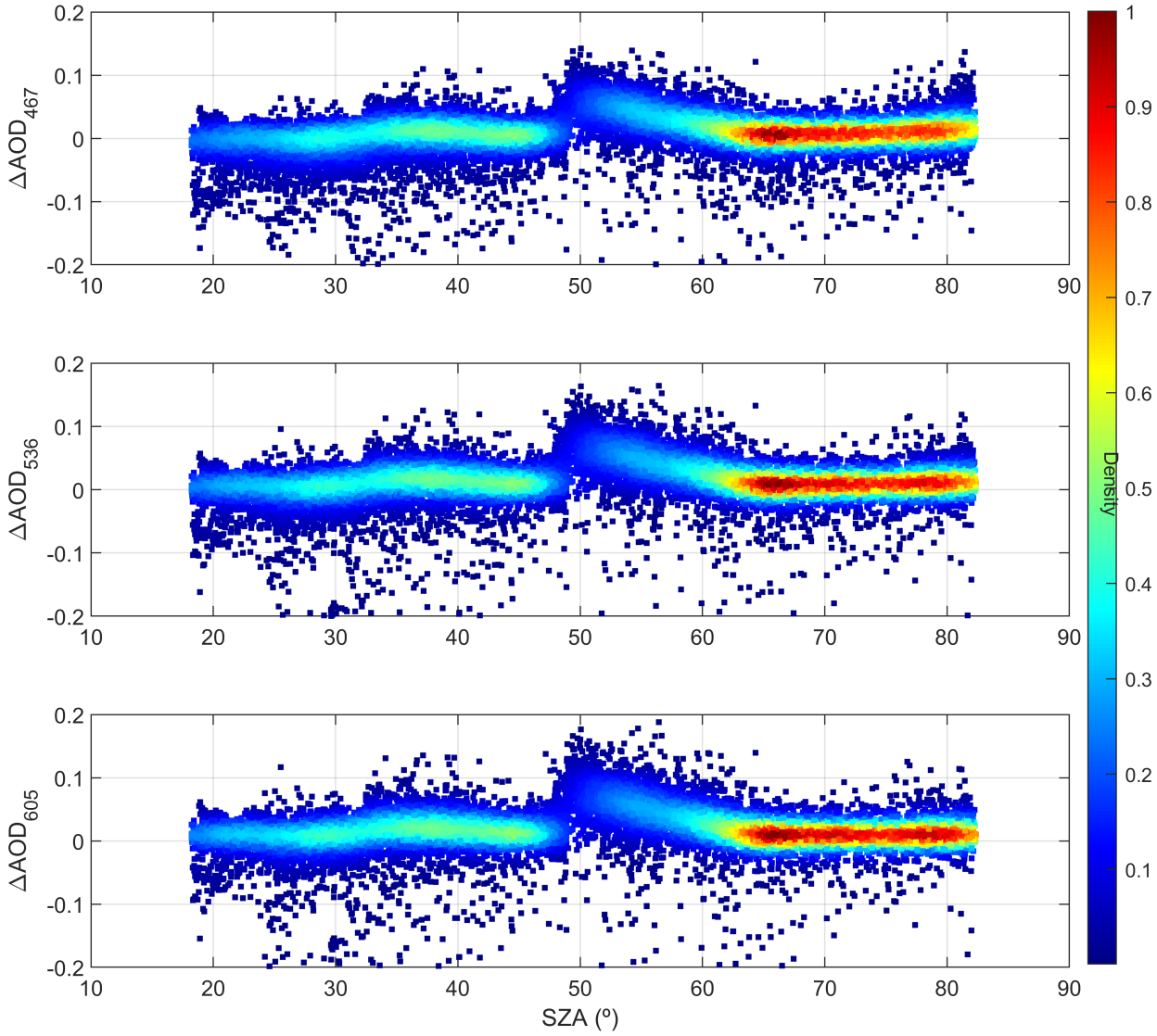

Figure S32. The Δ differences in the aerosol optical depth (AOD) retrieved by GRASP with the single-pixel approach (GRASP-CAM) and those obtained by AERONET at 467 nm (upper panel), 536 nm (middle panel) and 605 nm (bottom panel) as a function of the solar zenith angle (SZA). The retrievals not satisfying the criteria of at least one scattering angle leq14º are also included in the graphs. The colour legend represents the density of the plotted data points.

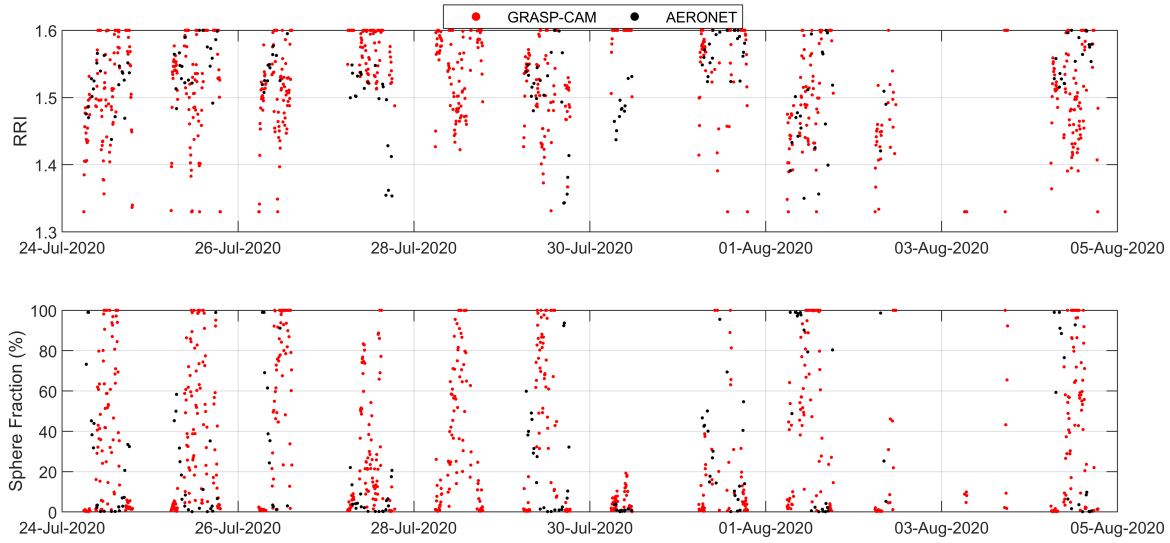

Figure S33. Real part of refractive index (RRI; upper panel) and the fraction of spherical particles (SPH; bottom panel) retrieved by GRASP with the single-pixel approach (GRASP-CAM) and by AERONET at Valladolid from 24 July 2020 to 4 August 2020. RRI from AERONET corresponds to the mean of the RRI at 440 and 675 nm.

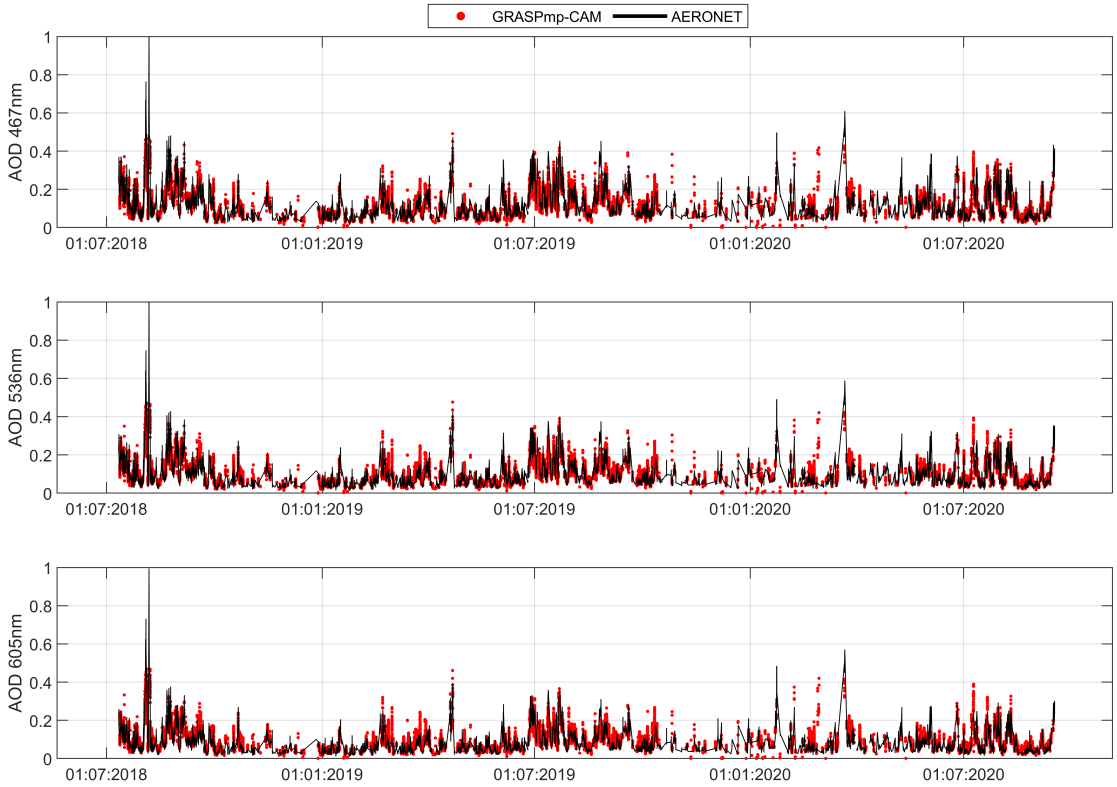

Figure S34. Aerosol optical depth (AOD) at 467 nm (upper panel), 536 nm (middle panel) and 605 nm (bottom panel) retrieved with the GRASP under multi-pixel approach (GRASPmp-CAM) and by AERONET at Valladolid from July 2018 to 15 September 2020.

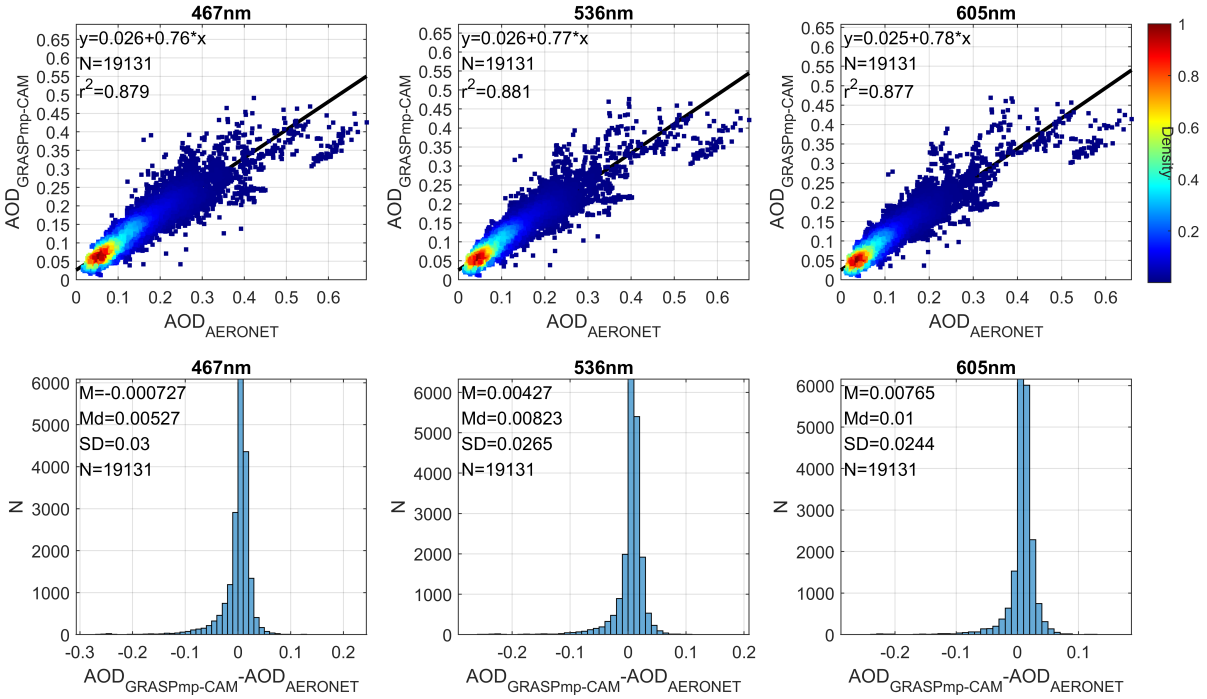

Figure S35. Upper panels) density scatter plots of the aerosol optical depth (AOD) retrieved by GRASP with the multi-pixel approach (GRASPmp-CAM) versus the AOD from AERONET at 467 nm (left panel), 536 nm (middle panel) and 605 nm (right panel); linear fit (black line) and its equation and the determination coefficient (r^2) are also shown. Bottom panels) Frequency histograms of the differences on AOD from GRASPmp-CAM and AERONET at 467 nm (left panel), 536 nm (middle panel) and 605 nm (right panel); The mean (M), median (Md) and standard deviation (SD) of these differences are also shown. Data obtained for solar zenith angle (SZA) values between 47.2º and 64.2º are not included.

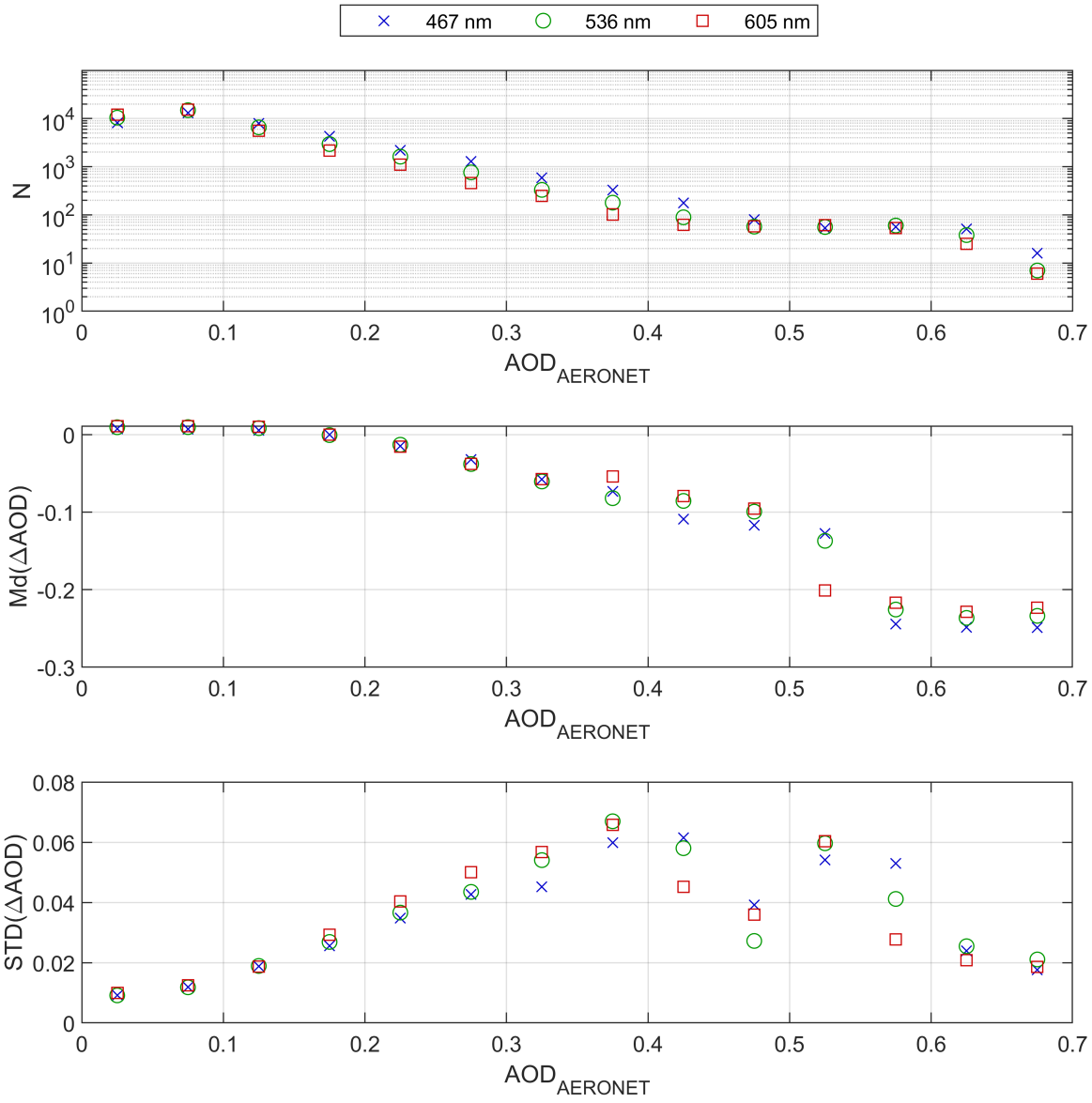

Figure S36. Median (Md; middle panel) and standard deviation (STD; bottom panel) of the Δ differences in the aerosol optical depth (AOD) retrieved by GRASP with the multi-pixel approach (GRASPmp-CAM) and those obtained by AERONET at 467, 536 and 605 nm for different AOD bins. The available amount of ΔAOD data (N) per AOD bin is also shown in upper panel for the three wavelengths. Data obtained for solar zenith angle (SZA) values between 47.2º and 64.2º are not included.

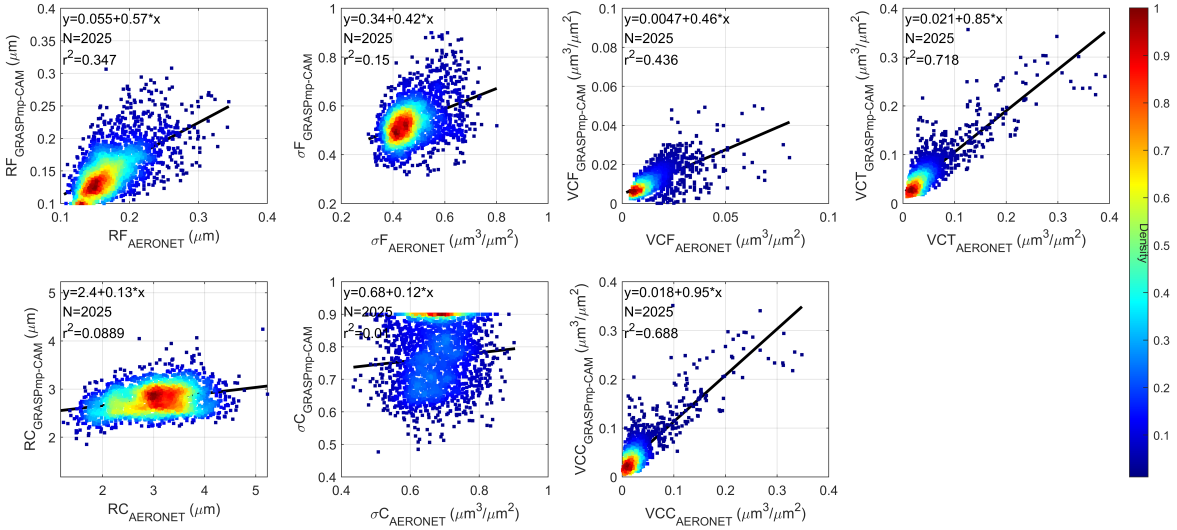

Figure S37. Density scatter plots of the aerosol size distribution properties retrieved by GRASP in multi-pixel approach (GRASPmp-CAM) versus the ones retrieved by AERONET; linear fit (black line) and its equation and the determination coefficient (r^2) are also shown. These size distribution properties are volume median radius of fine (RF) and coarse (RC) modes, standard deviation of log-normal distribution for fine (σF) and coarse (σC) modes, and aerosol volume concentration for fine (VCF) and coarse (VCC) modes and the total value (VCT). Data obtained for solar zenith angle (SZA) values between 47.2º and 64.2º are not included.

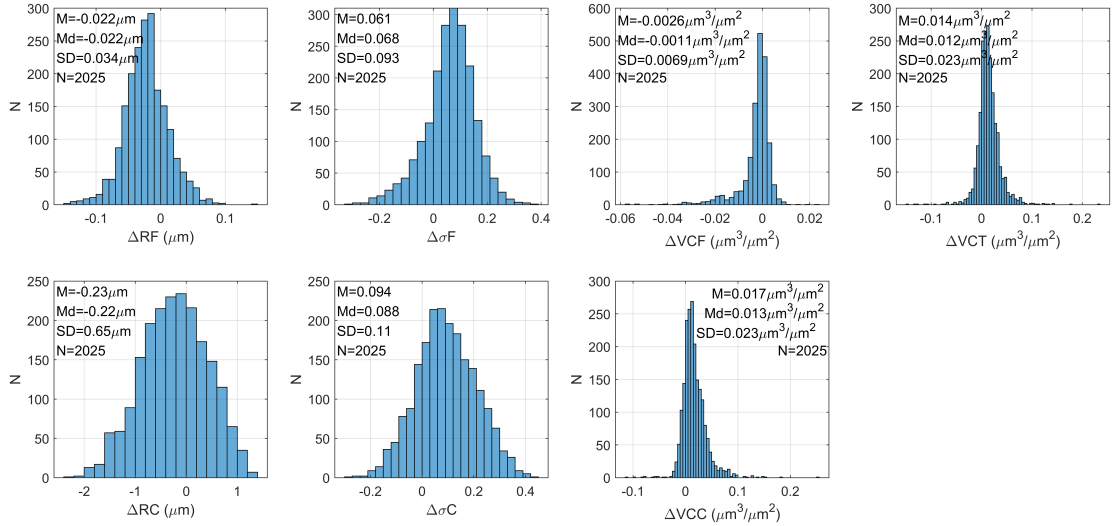

Figure S38. Frequency histograms of the Δ differences in the aerosol size distribution properties retrieved by GRASP with the multi-pixel approach (GRASPmp-CAM) and the ones retrieved by AERONET. The mean (M), median (Md) and standard deviation (SD) of these differences are also shown. These size distribution properties are: volume median radius of fine (RF) and coarse (RC) modes; standard deviation of log-normal distribution for fine (σF) and coarse (σC) modes; and aerosol volume concentration for fine (VCF) and coarse (VCC) modes and the total value (VC). Data obtained for solar zenith angle (SZA) values between 47.2º and 64.2º are not included.

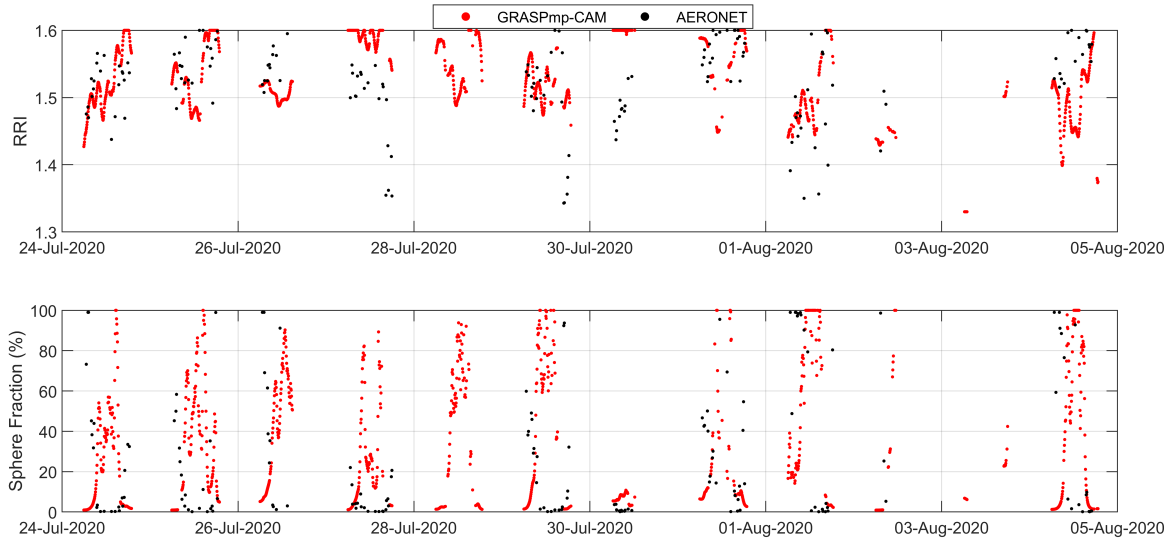

Figure S39. Real part of refractive index (RRI; upper panel) and the fraction of spherical particles (SPH; bottom panel) retrieved by GRASP with the multi-pixel approach (GRASPmp-CAM) and by AERONET at Valladolid from 24 July 2020 to 4 August 2020. RRI from AERONET corresponds to the mean of the RRI at 440 and 675 nm.